11 Non-Local Correlation Effects in Solids: Beyond DMFT

A.I. Lichtenstein and H. Hafermann
I. Institut für Theoretische Physik
Universität Hamburg

Contents

E. Pavarini, E. Koch, Dieter Vollhardt, and Alexander Lichtenstein
The LDA+DMFT approach to strongly correlated materials
Modeling and Simulation Vol. 1
Forschungszentrum Jülich, 2011, ISBN 978-3-89336-734-4
http://www.cond-mat.de/events/correl11

1 Introduction

The tremendous success of Dynamical Mean-Field Theory (DMFT) [1, 2] in understanding the Mott transition in simple model systems shows that the main correlation effects in fermionic lattices have a local character. Moreover realistic investigations of correlated materials within the LDA+DMFT scheme [3, 4, 5] also support the idea that the electronic structure of prototype Mott insulators, like V_2O_3, can be well understood within a local multi-orbital t_{2g} scheme. Nevertheless many interesting correlation effects in solid state physics, such as antiferromagnetic spin fluctuations, superconducting d-wave pairing, and many other phenomena have non-local character. In this Lecture we will discuss different ways to go beyond the DMFT approximation and include non-local correlations. There are two different approaches to non-local effects beyond the DMFT framework: one is based on numerical cluster DMFT extensions while another one is built on an analytical expansion around the local DMFT solution.

2 Cluster DMFT scheme

There are two groups of cluster DMFT extensions, which are formulated in real space (cellular DMFT – CDMFT) or in reciprocal space (Dynamical Cluster Approximation – DCA). We discuss first a simple model for the cluster DMFT scheme in real space which consists of a supercell in a two dimensional square lattice (Fig.1). Lower-case letters will be used for the original lattice vectors (x) and site indices (i, j), while upper-case will be reserved for supercell coordinates (X) and position of atoms in a supercell (I, J). Similarly, for wave vectors in original reciprocal lattice we will use (k) while for the reduced supercell Brillouin zone (K) will be used. The minimal cluster which allows us to investigate both antiferromagnetic (AFM) and superconducting (d-wave) order parameters on an equal footing consists of a 2×2 plaquette in an effective medium (see Fig.1).

The one band Hubbard model on the square lattice reads:

$$H = \sum_{ij\sigma} t_{ij} c^{\dagger}_{i\sigma} c_{j\sigma} + U \sum_{i} n_{i\uparrow} n_{i\downarrow}, \tag{1}$$

where t_{ij} are effective hopping parameters and U is the local Coulomb interaction. The exact Green function for the one-band Hubbard model (1) can be written in the following form

$$G(\mathbf{k}, i\omega) = (i\omega + \mu - t(\mathbf{k}) - \Sigma(\mathbf{k}, i\omega))^{-1}, \tag{2}$$

where $\omega = (2n+1)\pi/\beta, n = 0, \pm 1, ...$ are the Matsubara frequencies, β is the inverse temperature, μ the chemical potential, $t(\mathbf{k})$ the Fourier transform of the hopping parameters t_{ij}, and $\Sigma(\mathbf{k}, i\omega)$ is the non-local self-energy, which contains all information on single-particle correlations.

We can approximate the momentum-dependence of the self-energy in terms of a finite number of basis functions $\phi_i(\mathbf{k})$ [6]

$$\Sigma(\mathbf{k}, i\omega) \approx \sum_{i=1}^{N} \phi_i(\mathbf{k}) \Sigma_i(\omega) \tag{3}$$

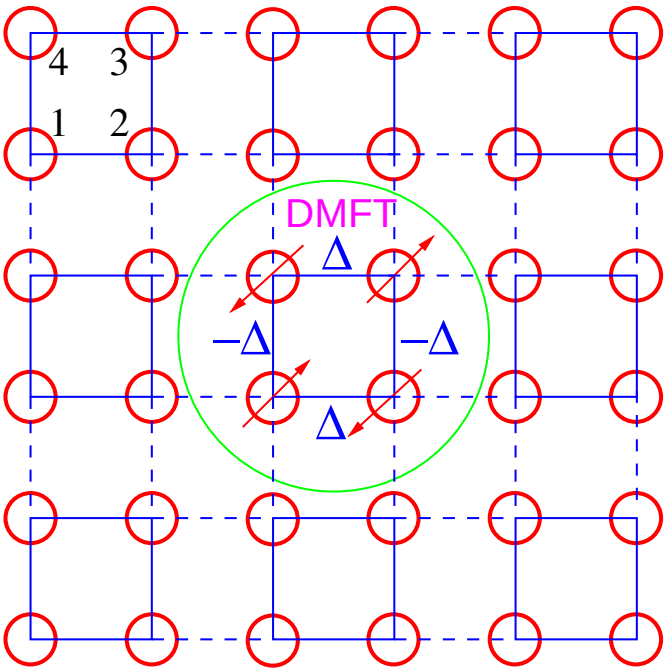

Fig. 1: *Schematic representation of the* 2×2 *supercell with antiferromagnetic and superconducting* d*-wave order parameters for cluster DMFT.*

In the most general scheme we can find $\Sigma_i(\omega)$ as a solution of a fictitious N-site quantum impurity model. Different cluster DMFT schemes differ in the choice of these basis functions. Numerical solutions of generalized multi-site quantum impurity models can be found within the recently developed continuous time Quantum Monte-Carlo scheme [7].
We introduce a "super-site" object as the 2×2 plaquette on a square lattice. The enumeration of the atoms inside the super-site is shown in the Fig. 1. A superspinor $C_I^\dagger = \{c_{I\alpha}^\dagger\}$ where $\alpha = 1, 2, 3, 4$ (including also the spin-indices) defines a super-fermionic operator for the I-th plaquette. The plaquette Green's function for the Hubbard model can be rewritten as

$$G\left(\mathbf{K}, i\omega\right) = \left[\left(i\omega + \mu\right)\mathbf{1} - T\left(\mathbf{K}\right) - \Sigma\left(i\omega\right)\right]^{-1} \tag{4}$$

where $T(\mathbf{K})$ is the effective hopping supermatrix, and $\mathbf{K}$ are the wave vectors within the reduced Brillouin zone, and $\Sigma\left(i\omega\right)$ is the self-energy supermatrix. For simplicity we will write all equations in the nearest-neighbor approximation, which means only one hopping in x- (t_x) and y- (t_y) direction. After supercell Fourier-transform we have the following expression for the supercell hopping matrix:

$$T_{I,J}\left(\mathbf{K}\right) = \begin{pmatrix} 0 & t_x K_x^+ & 0 & t_y K_y^+ \\ t_x K_x^- & 0 & t_y K_y^+ & 0 \\ 0 & t_y K_y^- & 0 & t_x K_x^- \\ t_y K_y^- & 0 & t_x K_x^+ & 0 \end{pmatrix} \tag{5}$$

where $K_{x(y)}^{\pm} \equiv 1 + \exp\left(\pm i K_{x(y)} a\right)$, a is the lattice constant, and each elements is a 2×2 matrix in spin space. Within the cluster DMFT approach we introduce the intra-atomic self-energy Σ_0

and inter-atomic self-energies Σ_x, Σ_y as well as the non-local self-energy Σ_{xy} in xy direction, which defines the local self-energy matrix for our 2×2 super-site:

$$\Sigma_{I,J}\left(i\omega\right) = \begin{pmatrix} \Sigma_0 & \Sigma_x & \Sigma_{xy} & \Sigma_y \\ \Sigma_x & \Sigma_0 & \Sigma_y & \Sigma_{xy} \\ \Sigma_{xy} & \Sigma_y & \Sigma_0 & \Sigma_x \\ \Sigma_y & \Sigma_{xy} & \Sigma_x & \Sigma_0 \end{pmatrix}$$

For a general $N \times N$ super-site impurity model (simp) the partition function can be written as a functional integral over the $2N$-component spin and site-dependent spinor Grassmann fields c^* and c :

$$Z = \int \mathcal{D}[c^*, c] e^{-S_{simp}}, \tag{6}$$

where

$$\begin{aligned} S_{simp} = -\sum_{I,J=0}^{N} \int_0^\beta d\tau \int_0^\beta d\tau' \; c^*_{I\sigma}(\tau) \left[\mathcal{G}^{-1}_\sigma(\tau - \tau')\right]_{IJ} c_{J\sigma}(\tau') \\ + \sum_{I=1}^{N} \int_0^\beta d\tau U n_{I,\uparrow}(\tau) n_{I,\downarrow}(\tau), \end{aligned} \tag{7}$$

where $\mathcal{G}$ is the $N \times N$ matrix of effective bath Green's function for a spin-collinear case.
The main problem of all cluster extension of DMFT is to find an optimal self-consistent way to obtain the bath Green's function matrix in imaginary time $\mathcal{G}_{IJ}(\tau - \tau')$ or in Matsubara space $\mathcal{G}_{IJ}(i\omega)$. In the free-cluster version of the CDMFT scheme [6] which is equivalent to the cellular DMFT method [8] or to the molecular CPA scheme in alloy theory [9] we can use the following prescription. First, we need to integrate out the superlattice degrees of freedom, similarly to the standard DMFT approach, and obtain the local Green's function matrix:

$$G_{IJ}\left(i\omega\right) = \sum_{\mathbf{K}} G_{IJ}\left(\mathbf{K}, i\omega\right), \tag{8}$$

where the summation runs over the reduced Brillouin zone of the plaquette superlattice.
Next we can write the matrix equation for the bath Green function matrix $\mathcal{G}$, which describes the effective interactions of the plaquette with rest of crystal. We use the impurity DMFT analogy, which allowed us to account for double-counting corrections for the local self-energy matrix: the bath Green function is not supposed to have any local self-energy contribution, since it comes later from the solution of the effective super-impurity problem (7). Therefore one needs to subtract the local self-energy contribution, which is equivalent to a solution of the following impurity problem, where all super-cites in Fig. 1 have the self-energy contributions, but not the "central-cluster":

$$\mathcal{G}^{-1}\left(i\omega\right) = G^{-1}\left(i\omega\right) + \Sigma\left(i\omega\right), \tag{9}$$

One can solve a complicated many-body problem described by super-impurity action Eq. (7). We can use the numerically exact continuous-time QMC scheme [7] and get the super-impurity

Green's function $G_{IJ}^{simp}(\tau) = -\langle c_{I\sigma}(\tau) c_{J\sigma}^{\dagger}(0)\rangle_{simp}$. The new cluster-local self-energy is equal to the difference of the inverse input and output Green's functions of this local many-body problem:

$$\Sigma_{new}(i\omega) = \mathcal{G}^{-1}(i\omega) - G_{simp}^{-1}(i\omega). \tag{10}$$

Finally, we can close the CDMFT self-consistent loop for the cluster self-energy $\Sigma_{I,J}(i\omega)$ by using in the next iterations the new self-energy from Eq. (10) in the super-lattice Hamiltonian from Eq. (1). The CDMFT self-consistency condition reads:

$$G_{IJ}^{simp}(i\omega) = G_{IJ}(i\omega). \tag{11}$$

In fact this CDMFT scheme is equivalent to the multi-orbital LDA+DMFT approach [4], where the super-site indices (I, J) play the role of different orbitals (m, m'). A crucial difference is related to the fact, that multi-orbital DMFT does not break the translational symmetry of original lattice, while the standard CDMFT scheme [8, 6] does lower the symmetry of lattice due to the local form of the super-site self-energy Eq. (7). The present "matrix" form of CDMFT with non-periodic self-energy allows us to study multicomponent order parameters (Fig. 1). In this case we have the standard DMFT problem with four "orbital" states per super-site. We use the generalized Gorkov-Nambu technique to analyze the coexistence of magnetic ordering and superconductivity. Let us introduce the superspinor

$$\Psi_I^{+}(\tau) = \left(c_{I\uparrow}^{\dagger}, c_{I\downarrow}^{\dagger}, c_{I\uparrow}, c_{I\downarrow}\right) \tag{12}$$

and the anomalous averages describing the (collinear) antiferromagnetism $\left\langle c_{I\uparrow}^{\dagger} c_{J\downarrow} \right\rangle$ and the superconductivity $\Delta_{IJ} = \langle c_{I\downarrow} c_{J\uparrow}\rangle$.

One may realize that the cellular DMFT approximation is not very suitable for the superconducting d-wave order parameter since Δ is located on the bonds as depicted in Fig. (1). Therefore one can lose half of the superconducting bonds and reduce approximately by a factor of two the HTSC transition temperature. We can also formulate a "periodic" CDMFT scheme by renormalizing the hopping with the cluster self-energy [6].

The effective Hamiltonian defined through the translationally invariant (**k**-dependent) self-energy corresponds to the renormalized energy dependent hoppings: $t_x = t + \Sigma_x$, $t_y = t + \Sigma_y$. The functions $\Sigma_0(i\omega)$, $\Sigma_x(i\omega)$, $\Sigma_y(i\omega)$ are found self-consistently within the cluster DMFT scheme [6] and for the d-wave superconducting state $\Sigma_x \neq \Sigma_y$. It is straightforward to generalize this scheme for a next-nearest neighbor hopping as well as the long-range Green function and the self-energy. In this case we can renormalize also the second-nearest hopping: $t_{xy} = t' + \Sigma_{xy}$ for the 2×2 cluster. The local cluster Green matrix in this case is equal to $G_{ij}(i\omega) = \sum_{\mathbf{k}} G_{ij}(\mathbf{k}, i\omega)$, and the summation runs over the original Brillouin zone of the square lattice. Unfortunately we can not prove that this periodic CDMFT scheme is causal. Later we will discuss different ways of obtaining a periodic self-energy within CDMFT.

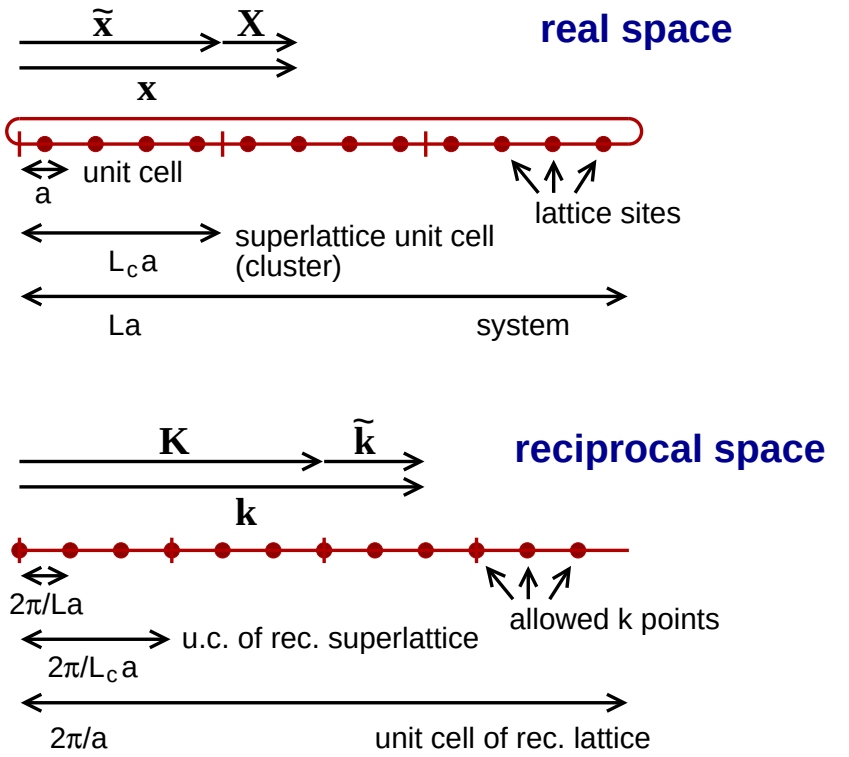

Fig. 2: *Decomposition of real-space lattice vectors, $\boldsymbol{x} = \boldsymbol{X} + \widetilde{\boldsymbol{x}}$, and reciprocal-space wave vectors, $\boldsymbol{k} = \widetilde{\boldsymbol{k}} + \boldsymbol{K}$, for a $D = 1$ dimensional lattice (lattice constant a) with $L = 12$ sites tiled with $L/L_c = 3$ clusters consisting of $L_c = 4$ sites each. $\boldsymbol{x}$: original lattice. $\widetilde{\boldsymbol{x}}$: superlattice. $\boldsymbol{X}$: sites in a cluster. Reciprocal space: There are L allowed wave vectors $\boldsymbol{k}$ in the unit cell of the lattice reciprocal to $\boldsymbol{x}$, and there are L/L_c allowed wave vectors $\widetilde{\boldsymbol{k}}$ in the unit cell of the lattice reciprocal to the superlattice $\widetilde{\boldsymbol{x}}$. $\boldsymbol{K}$ are the reciprocal superlattice vectors, $\exp(i\boldsymbol{K}\widetilde{\boldsymbol{x}}) = 1$. From Ref. [19].*

3 Dynamical cluster approximation: general consideration

We start discussion of dynamical cluster approaches in reciprocal space with introducing some notations (see Fig. 2) (for a review, see Ref. [10]). The cluster need not be a physical subsystem of the original lattice [11, 12, 13]. We consider a system on a D-dimensional lattice of L sites with periodic boundary conditions and $L \to \infty$ in the end. The position vector to a site in the lattice is denoted by $\boldsymbol{x}$. There are L allowed wave vectors in a unit cell of the reciprocal lattice which are denoted by $\boldsymbol{k}$. The lattice is tiled with L/L_c clusters consisting of L_c sites each. Let $\widetilde{\boldsymbol{x}}$ be the position vector of the cluster origin, and $\boldsymbol{X}$ the position vector of a site in a cluster, referring to the cluster origin. We then have the unique decomposition $\boldsymbol{x} = \boldsymbol{X} + \widetilde{\boldsymbol{x}}$. The vectors $\widetilde{\boldsymbol{x}}$ form a superlattice with a unit-cell volume enlarged by the factor L_c. In a unit cell of the reciprocal superlattice there are L/L_c allowed wave vectors $\widetilde{\boldsymbol{k}}$. Its volume is reduced by the factor L_c as compared to the volume of the reciprocal unit cell of the original lattice. For a given $\boldsymbol{k}$ we have the unique decomposition $\boldsymbol{k} = \widetilde{\boldsymbol{k}} + \boldsymbol{K}$ where $\boldsymbol{K}$ are the vectors of the reciprocal superlattice, i.e. $\exp(i\boldsymbol{K}\widetilde{\boldsymbol{x}}) = 1$. In the reciprocal unit cell of the original lattice, there are L_c vectors $\boldsymbol{K}$. These can also be interpreted as the allowed cluster wave vectors when imposing

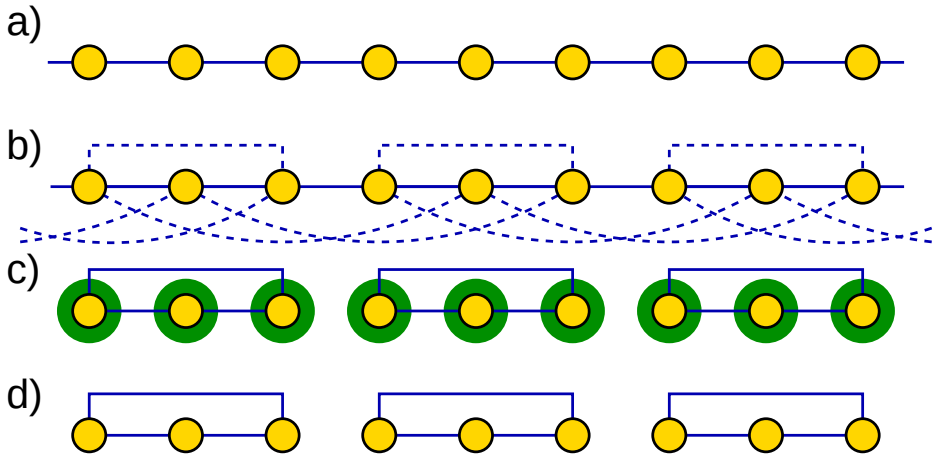

Fig. 3: *a) Hubbard 1d-model. b) The original Hubbard model but with a modified one-particle part $\boldsymbol{t} \rightarrow \overline{\boldsymbol{t}}$ which is the starting point for the dynamical cluster approximation (DCA). $\overline{\boldsymbol{t}}$ is invariant under superlattice and cluster translations. c) Reference system generating the DCA. Note that $\boldsymbol{t}'$ has the same translational symmetries as $\overline{\boldsymbol{t}}$. d) Reference system generating a simplified DCA. From Ref. [19].*

periodic boundary conditions on the individual cluster.
In the following we consider the $L \times L$ matrix $\boldsymbol{U}$ with elements

$$U_{\boldsymbol{x},\boldsymbol{k}} = \frac{1}{\sqrt{L}} e^{i\boldsymbol{k}\boldsymbol{x}} \,, \tag{13}$$

and the $L/L_c \times L/L_c$ matrix $\boldsymbol{V}$ with elements

$$V_{\widetilde{\boldsymbol{x}},\widetilde{\boldsymbol{k}}} = \frac{1}{\sqrt{L/L_c}} e^{i\widetilde{\boldsymbol{k}}\widetilde{\boldsymbol{x}}} \,, \tag{14}$$

and the $L_c \times L_c$ matrix $\boldsymbol{W}$ with elements

$$W_{\boldsymbol{X},\boldsymbol{K}} = \frac{1}{\sqrt{L_c}} e^{i\boldsymbol{K}\boldsymbol{X}} \,. \tag{15}$$

Notes, that $\boldsymbol{U}$, $\boldsymbol{V}$ and $\boldsymbol{W}$ are unitary and define Fourier transformations between the respective real and reciprocal spaces. It is obvious, that $\boldsymbol{U} \neq \boldsymbol{V}\boldsymbol{W} = \boldsymbol{W}\boldsymbol{V}$:

$$U_{\boldsymbol{x},\boldsymbol{k}} = \frac{1}{\sqrt{L}} e^{i\boldsymbol{k}\boldsymbol{x}} = \frac{1}{\sqrt{L}} e^{i(\widetilde{\boldsymbol{k}}\boldsymbol{X}+\widetilde{\boldsymbol{k}}\widetilde{\boldsymbol{x}}+\boldsymbol{K}\boldsymbol{X})} \neq \frac{1}{\sqrt{L}} e^{i(\widetilde{\boldsymbol{k}}\widetilde{\boldsymbol{x}}+\boldsymbol{K}\boldsymbol{X})} = V_{\widetilde{\boldsymbol{x}},\widetilde{\boldsymbol{k}}} W_{\boldsymbol{X},\boldsymbol{K}} \,. \tag{16}$$

A hopping $t_{\boldsymbol{x},\boldsymbol{x}'}$ which is invariant under lattice translations $\boldsymbol{x}_0$, i.e. $t_{\boldsymbol{x}+\boldsymbol{x}_0,\boldsymbol{x}'+\boldsymbol{x}_0} = t_{\boldsymbol{x},\boldsymbol{x}'}$, is diagonalized by normal Fourier transformations $\boldsymbol{U}$: $(\boldsymbol{U}^\dagger \boldsymbol{t} \boldsymbol{U})_{\boldsymbol{k}\boldsymbol{k}'} = t(\boldsymbol{k})\delta_{\boldsymbol{k},\boldsymbol{k}'}$. By definition, the one-electron spectrum is just Fourier transform of the hopping matrix elements: $\varepsilon_{\boldsymbol{k}} \equiv t(\boldsymbol{k})$. A quantity $T_{\boldsymbol{x},\boldsymbol{x}'}$ which is invariant under superlattice translations $\widetilde{\boldsymbol{x}}_0$ as well as under cluster translations $\boldsymbol{X}_0$ (i.e. which is cyclic on the cluster), $T_{\boldsymbol{x}+\widetilde{\boldsymbol{x}}_0,\boldsymbol{x}'+\widetilde{\boldsymbol{x}}_0} = T_{\boldsymbol{x}+\boldsymbol{X}_0,\boldsymbol{x}'+\boldsymbol{X}_0} = T_{\boldsymbol{x},\boldsymbol{x}'}$, is diagonalized by alternative DCA-transformation $\boldsymbol{V}\boldsymbol{W}$: $(\boldsymbol{W}^\dagger \boldsymbol{V}^\dagger \boldsymbol{T} \boldsymbol{V}\boldsymbol{W})_{\widetilde{\boldsymbol{k}}\boldsymbol{K},\widetilde{\boldsymbol{k}}'\boldsymbol{K}'} = T(\widetilde{\boldsymbol{k}},\boldsymbol{K})\delta_{\widetilde{\boldsymbol{k}},\widetilde{\boldsymbol{k}}'}\delta_{\boldsymbol{K},\boldsymbol{K}'}$. Following Refs. [15, 16, 19], we introduce a fictitious hopping which corresponds to the real-space formulation of the DCA-scheme:

$$\overline{\boldsymbol{t}} = (\boldsymbol{V}\boldsymbol{W})\boldsymbol{U}^\dagger \, \boldsymbol{t} \, \boldsymbol{U}(\boldsymbol{V}\boldsymbol{W})^\dagger \,, \tag{17}$$

which is just the DCA Fourier back-transform of the one-electron spectrum $\varepsilon_{\boldsymbol{k}}$. For clusters of finite size L_c, the combined Fourier transformation $\boldsymbol{VW}$ is different from $\boldsymbol{U}$. For $L_c \to \infty$, however, this becomes irrelevant. With $\varepsilon(\boldsymbol{k}) = (\boldsymbol{U}^\dagger \boldsymbol{t} \boldsymbol{U})(\boldsymbol{k})$ we have:

$$\overline{t}_{\boldsymbol{x}\boldsymbol{x}'} = \frac{1}{L_c} \sum_{\boldsymbol{K}} e^{i\boldsymbol{K}(\boldsymbol{X}-\boldsymbol{X}')} \frac{L_c}{L} \sum_{\widetilde{\boldsymbol{k}}} e^{i\widetilde{\boldsymbol{k}}(\widetilde{\boldsymbol{x}}-\widetilde{\boldsymbol{x}}')} \varepsilon(\widetilde{\boldsymbol{k}} + \boldsymbol{K}) \,. \tag{18}$$

Obviously, $\overline{\boldsymbol{t}}$ is invariant under superlattice translations as well as under cluster translations (with periodic cluster boundary conditions). The original and the modified system are represented by Fig. 3a, b. The construction of $\overline{\boldsymbol{t}}$ is such that it exhibits the same translational symmetries as the one-particle parameters $\boldsymbol{t}'$ of a reference system consisting of isolated clusters tiling the original lattice with periodic boundary conditions, see Fig. 3c, d. Since both, $\boldsymbol{t}$ and $\overline{\boldsymbol{t}}$, are invariant under superlattice translations, we can compare $t_{\boldsymbol{X}\boldsymbol{X}'}(\widetilde{\boldsymbol{k}}) = (\boldsymbol{V}^\dagger \boldsymbol{t} \boldsymbol{V})_{\boldsymbol{X}\boldsymbol{X}'}(\widetilde{\boldsymbol{k}})$ with $\overline{t}_{\boldsymbol{X}\boldsymbol{X}'}(\widetilde{\boldsymbol{k}}) = (\boldsymbol{V}^\dagger \overline{\boldsymbol{t}} \boldsymbol{V})_{\boldsymbol{X}\boldsymbol{X}'}(\widetilde{\boldsymbol{k}})$. It turns out they are equal up to a phase factor:

$$\begin{aligned}
\overline{t}_{\boldsymbol{X}\boldsymbol{X}'}(\widetilde{\boldsymbol{k}}) &= \frac{1}{L_c} \sum_{\boldsymbol{K}} e^{i\boldsymbol{K}(\boldsymbol{X}-\boldsymbol{X}')} \varepsilon(\widetilde{\boldsymbol{k}} + \boldsymbol{K}) \\
&= \frac{L_c}{L} \sum_{\widetilde{\boldsymbol{x}}\widetilde{\boldsymbol{x}}'} e^{-i\widetilde{\boldsymbol{k}}(\widetilde{\boldsymbol{x}}+\boldsymbol{X}-\widetilde{\boldsymbol{x}}'-\boldsymbol{X}')} t_{\widetilde{\boldsymbol{x}}+\boldsymbol{X},\widetilde{\boldsymbol{x}}'+\boldsymbol{X}'} \\
&= e^{-i\widetilde{\boldsymbol{k}}(\boldsymbol{X}-\boldsymbol{X}')} t_{\boldsymbol{X}\boldsymbol{X}'}(\widetilde{\boldsymbol{k}}) \,.
\end{aligned} \tag{19}$$

The main idea of the DCA is to restore momentum conservation within the cluster by a rescale the effective hoppings. In CDMFT, the intracluster transform of the dispersion given by the super-cell Fourier sum:

$$\mathbf{t}_{\mathbf{X},\mathbf{X}'}(\tilde{\mathbf{k}}) = \frac{1}{L_{\mathrm{c}}} \sum_{\mathbf{K}} e^{i(\mathbf{K}+\tilde{\mathbf{k}})(\mathbf{X}-\mathbf{X}')} \epsilon_{\mathbf{K}+\tilde{\mathbf{k}}}, \tag{20}$$

while in the DCA, an addition phase factors $e^{i\tilde{\mathbf{k}}\mathbf{X}}$ are excluded using the transform (see Eq. (19)).

$$\overline{t}_{\mathbf{X},\mathbf{X}'}(\tilde{\mathbf{k}}) = \mathbf{t}_{\mathbf{X},\mathbf{X}'}(\tilde{\mathbf{k}}) e^{-i\tilde{\mathbf{k}}(\mathbf{X}-\mathbf{X}')} = \frac{1}{L_{\mathrm{c}}} \sum_{\mathbf{K}} e^{i\mathbf{K}(\mathbf{X}-\mathbf{X}')} \epsilon_{\mathbf{K}+\tilde{\mathbf{k}}}. \tag{21}$$

The intracluster hopping in DCA is therefore given by the intracluster Fourier transform of the dispersion Eq. (21), which is obvious by coarse-graining . This gives the DCA Green's function which is diagonal in cluster Fourier space:

$$G(\mathbf{K}+\tilde{\mathbf{k}}, i\omega) = \frac{1}{i\omega + \mu - \varepsilon(\mathbf{K}+\tilde{\mathbf{k}}) - \Sigma(\mathbf{K}, i\omega)}. \tag{22}$$

The self-energy becomes a piecewise constant function in the k-space [10]. Finally, the self-consistent condition for $\Sigma(\mathbf{K}, i\omega)$ in the DCA-scheme is similar to the CDMFT one Eq. (11):

$$G^{imp}(\mathbf{K}, i\omega) = G(\mathbf{K}, i\omega) \equiv \sum_{\tilde{\mathbf{k}}} G(\mathbf{K}+\tilde{\mathbf{k}}, i\omega). \tag{23}$$

We can also try to 'periodize' the cluster-DMFT scheme [6, 15]. The CDMFT violates translational invariance with respect to the cluster sites. This is obvious for clusters with $L_\mathrm{c} \geq 3$, where bulk and surface sites of a cluster may be distinguished. The CDMFT calculations are carried out in the cluster real-space representation (i.e. all quantities are matrices in the cluster sites), since there is no benefit in changing to the cluster k-space representation, which is not diagonal.

Since translational invariance is broken, the lattice quantities are functions of two independent momenta $\mathbf{k}$ and $\mathbf{k}'$. They can differ by a reciprocal lattice vector $\mathbf{Q}$, where $Q_i = 0, \ldots, (L_\mathrm{c} - 1)2\pi/L_\mathrm{c}$. The self-energy can be expressed in terms of the cluster self-energy as

$$\Sigma(\mathbf{k}, \mathbf{k}', i\omega) = \frac{1}{L_\mathrm{c}} \sum_{\mathbf{Q}} \sum_{\mathbf{X},\mathbf{X}'} e^{i\mathbf{k}\mathbf{X}} \Sigma_\mathrm{c}(\mathbf{X}, \mathbf{X}', i\omega) e^{-i\mathbf{k}'\mathbf{X}'} \delta(\mathbf{k} - \mathbf{k}' - \mathbf{Q}), \tag{24}$$

where the dependence on cluster sites is written explicitly. A translationally invariant solution is obtained by approximating the lattice quantities only by the $\mathbf{Q} = 0$ contribution:

$$\Sigma(\mathbf{k}, i\omega) = \frac{1}{L_\mathrm{c}} \sum_{\mathbf{X},\mathbf{X}'} = e^{i\mathbf{k}(\mathbf{X}-\mathbf{X}')} \Sigma_\mathrm{c}(\mathbf{X}, \mathbf{X}', i\omega). \tag{25}$$

Transforming back to real space shows that the lattice quantities for a given distance $\mathbf{x} - \mathbf{x}'$ are obtained as an average over the cluster quantities for the same distance,

$$\Sigma(\mathbf{x} - \mathbf{x}', i\omega) = \frac{1}{L_\mathrm{c}} \sum_{\mathbf{X},\mathbf{X}'} \Sigma_\mathrm{c}(\mathbf{X}, \mathbf{X}', i\omega)\, \delta_{\mathbf{X}-\mathbf{X}',\mathbf{x}-\mathbf{x}'}. \tag{26}$$

Spatial correlations are hence included up to a length determined by the extension of the cluster. Note that Eq. (26) underestimates the nonlocal contributions, in particular for small clusters. Using the shorthand notation $\Sigma_{\mathbf{X},\mathbf{X}'} = \Sigma(\mathbf{X}, \mathbf{X}')$, one sees that the local self-energy is averaged correctly, $\Sigma(x = 0) = (\Sigma_{\mathrm{c}\,00} + \Sigma_{\mathrm{c}\,11})/2$, while the nearest-neighbor self-energy contribution according to (26) would read $\Sigma(x = 1) = (1/2)\Sigma_{\mathrm{c}\,10}$, since $\Sigma_{\mathrm{c}\,01}$ contributes to $\Sigma(x = -1)$. It was therefore suggested to reweigh the terms in the sum [15]. For the above example, $\Sigma(x = 1) = \Sigma_{\mathrm{c}\,10}$.

When translational invariance is recovered in this way, the solution of the lattice problem may be viewed as shown in Fig. 4: The lattice is replaced by a lattice of clusters all of which are embedded in a self-consistent bath. The self-energy on a cluster is obtained from the self-consistent solution of the local problem and the intercluster self-energy between sites on neighboring clusters at a distance $\mathbf{x} - \mathbf{x}'$ is artificially set equal to the average of the intracluster self-energy for the same distance. The self-energy for distances exceeding the maximum distance between sites within the cluster is zero.

Following Ref. [17] we can compare the CDMFT and DCA schemes for the linear 3-cite cluster from Fig. (3). Writing the single-electron part of Hamiltonian as the supercell matrix $\mathbf{T}(\tilde{\mathbf{k}})$, the average cluster hopping is given by

$$\mathbf{T}_c = \int d\tilde{\mathbf{k}}\, \mathbf{T}(\tilde{\mathbf{k}})\,. \tag{27}$$

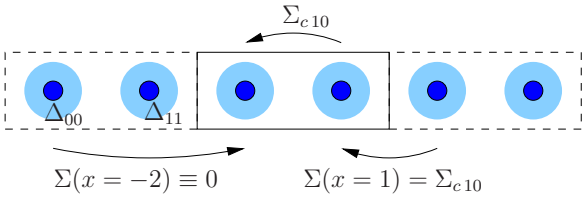

Fig. 4: *Illustration of the CDMFT lattice self-energy. The original lattice is replaced by a collection of clusters embedded in a self-consistent bath. The intercluster self-energy* $\Sigma(x=1)$ *is approximated by the intracluster self-energy* $\Sigma_{c\,10}$ *for this distance not exceeding the maximal distance between cluster sites and zero otherwise. From the Ref. [14].*

The interaction terms are simply those of Eq. (1), restricted to the cluster.
The Hamiltonian $H(\tilde{\mathbf{k}})$ in the reciprocal space of the super-lattice $\{\tilde{\mathbf{x}}\}$ of clusters can be obtained by changing to the basis of fermionic-operators in Eq.(1):

$$\tilde{c}^{\mathrm{CDMFT}}_{\mathbf{X},\sigma}(\tilde{\mathbf{k}}) = \sum_{\tilde{\mathbf{x}}} e^{-i\tilde{\mathbf{k}}\tilde{\mathbf{x}}}\, c_{\tilde{\mathbf{x}}+\mathbf{X},\sigma}\,. \tag{28}$$

The resulting quantum cluster approximation is the CDMFT. Alternatively, we can start from the operators in the reciprocal space of the *lattice* to obtain

$$\tilde{c}^{\mathrm{DCA}}_{\mathbf{X},\sigma}(\tilde{\mathbf{k}}) = \sum_{\tilde{\mathbf{x}}} e^{-i\tilde{\mathbf{k}}(\tilde{\mathbf{x}}+\mathbf{X})}\, c_{\tilde{\mathbf{x}}+\mathbf{X},\sigma} \equiv= \sum_{\tilde{\mathbf{x}}} e^{-i(\tilde{\mathbf{k}}\tilde{\mathbf{x}}+\phi(\tilde{\mathbf{k}},\tilde{\mathbf{x}}))}\, c_{\tilde{\mathbf{x}}+\mathbf{X},\sigma}\,. \tag{29}$$

The choice of the operators in the two approaches differs just by local phase factors $\phi(\tilde{\mathbf{k}},\tilde{\mathbf{x}})$ [17]. In the CDMFT this gauge is chosen such that phases appear only in matrix elements involving different clusters. Thus all matrix elements on the cluster are the same as in the original Hamiltonian. The price for retaining the original matrix elements on the cluster is a breaking of the translation-symmetry of the original lattice. The DCA-scheme opts instead to retain this symmetry by distributing the phase change uniformly over the cluster-sites. The price for retaining translation-invariance is that the matrix elements in the cluster Hamiltonian differ from those in the original Hamiltonian. In both cases, CDMFT and DCA, the eigenvalues of $\mathbf{T}(\tilde{\mathbf{k}})$ are identical to the eigenvalues of the non-interacting part of H.
In the CDMFT gauge we have we have for a three-site cluster ($L_c = 3$) in 1-d lattice [17] :

$$\mathbf{T}^{CDMFT}(\tilde{k}) = t \begin{pmatrix} 0 & 1 & e^{-3i\tilde{k}} \\ 1 & 0 & 1 \\ e^{3i\tilde{k}} & 1 & 0 \end{pmatrix} \tag{30}$$

so that $\mathbf{T}_c$ is the original single-electron Hamiltonian restricted to the cluster:

$$\mathbf{T}_c^{CDMFT} = \frac{3}{2\pi}\int_{-\pi/3}^{\pi/3} d\tilde{k}\, \mathbf{T}(\tilde{k}) = t \begin{pmatrix} 0 & 1 & 0 \\ 1 & 0 & 1 \\ 0 & 1 & 0 \end{pmatrix}\,. \tag{31}$$

In the DCA gauge for 3-cite linear cluster we have

$$\mathbf{T}^{DCA}(\tilde{k}) = t \begin{pmatrix} 0 & e^{i\tilde{k}} & e^{-i\tilde{k}} \\ e^{-i\tilde{k}} & 0 & e^{i\tilde{k}} \\ e^{i\tilde{k}} & e^{-i\tilde{k}} & 0 \end{pmatrix} . \tag{32}$$

Now the $\mathbf{T_c}$ matrix is cyclic and has translation symmetry (see Fig.(3 c)), but rescaled hopping matrix elements:

$$\mathbf{T}_c^{DCA} = \frac{3}{2\pi} \int_{\pi/3}^{\pi/3} d\tilde{k}\, \mathbf{T}(\tilde{k}) = \frac{3\sqrt{3}}{2\pi}\, t \begin{pmatrix} 0 & 1 & 1 \\ 1 & 0 & 1 \\ 1 & 1 & 0 \end{pmatrix} . \tag{33}$$

This effective rescaling of the hopping parameters in DCA-scheme can lead to a problem with investigations of complex band structure effects, such as an extended van Hove singularities [32]. We note also that the similar consideration apply to the variational cluster approach [11], which is based on the self-energy functional theory [18, 19].

4 Symmetry properties of the cluster scheme

Let us discuss a symmetry properties of paramagnetic solution of culster extension of DMFT in the simple case of 2- and 4-site clusters [20]. In Fig. Fig. (5) the simplest 2-site and 4-site tiling on square and cubic lattices plotted. For each quantity, like Green's function G, self energy Σ, and bath function $\mathcal{G}$, there are momentum and real-space components labeled by some subscript. In this paper, the real-space component is labeled by a number (0 - on-site, 1 - nearest neighbor, etc.) while the momentum-space sectors labelled by capital letters (S, P, D).

4.1 Formalism for the 2-site cluster method

Now we apply general cluster formalism to specific cases, first to the 2-site cluster in the square lattice. The solution of 2-site impurity problem gives the following matrix Green function:

$$\hat{G}^{imp} = \begin{pmatrix} G_0 & G_1 \\ G_1 & G_0 \end{pmatrix} \quad \hat{\Sigma}^{imp} = \begin{pmatrix} \Sigma_0 & \Sigma_1 \\ \Sigma_1 & \Sigma_0 \end{pmatrix} \tag{34}$$

The partitioning of Brillouin zone in this case is given in Fig(5), so two $\mathbf{K}$ points according to this division is $\mathbf{K}_I = 0$, $\mathbf{K}_{II} = (\pi, \pi)$. We label region I and II or S and P sectors. Corresponding to $\mathbf{K}_I$ and $\mathbf{K}_{II}$, one gets $\mathbf{R}_0 = 0$ and $\mathbf{R}_1 = (\pm 1, 0)$ or $(0, \pm 1)$. The lattice self energy is related to $\hat{\Sigma}^{imp}$ by

$$\Sigma_{DCA}(\vec{k}, \omega) = \begin{cases} \Sigma_S^{imp} = \Sigma_0 + \Sigma_1 & \text{for } \mathbf{k} \in \text{Region } I(S) \\ \Sigma_P^{imp} = \Sigma_0 - \Sigma_1 & \text{for } \mathbf{k} \in \text{Region } II(P) \end{cases} \tag{35}$$

The partial density of states are

$$D_{S(P)}(\epsilon) = 2 \times \int_{\mathbf{k} \in I(II)} d\mathbf{k}\ \delta(\epsilon - \epsilon_{\mathbf{k}}) \tag{36}$$

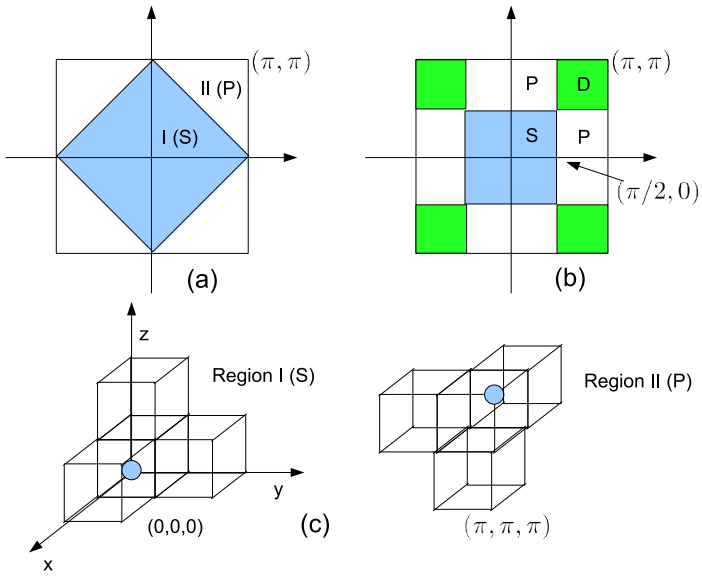

Fig. 5: *Partition of the Brillouin zone. (a) 2-site DCA on square lattice. (b) 4-site DCA on square lattice. (c) 2-site DCA on cubic lattice From Ref.[20].*

and the self-consistency equation is

$$\begin{aligned} G_0 &= (G_S + G_P)/2 \\ G_1 &= (G_S - G_P)/2 \end{aligned} \tag{37}$$

with

$$G_{S(P)} = \int \frac{D_{S(P)}(\epsilon)\ d\epsilon}{\omega + \mu - \epsilon_{\mathbf{k}} - (\Sigma_0 \pm \Sigma_1)} \tag{38}$$

4.2 Formalism for the 4-site cluster method

In the 4-site cluster the Brillouin zone is divided into four sectors which are labelled as S, P, and D, as shown in Fig(5). Four $\mathbf{K}$ points are $(0,0)$ $(\pi,0)$ $(0,\pi)$ (π,π) leading to four $\mathbf{R}$ as $(0,0)$ $(1,0)$ $(0,1)$ $(1,1)$. The partial DOS is defined as

$$D^{(4)}_{S(P,D)}(\epsilon) = 4 \times \int_{\mathbf{k}\in S(P,D)} d\mathbf{k}\ \delta(\epsilon - \epsilon_{\mathbf{k}}) \tag{39}$$

where the superscript (4) is used to distinguish from the partial DOS in 2-site DCA (see Fig(6)). After solving a 4-site impurity cluster problem, in the disordered phase one gets

$$\hat{G}^{imp} = \begin{pmatrix} G_0 & G_1 & G_2 & G_1 \\ G_1 & G_0 & G_1 & G_2 \\ G_2 & G_1 & G_0 & G_1 \\ G_1 & G_2 & G_1 & G_0 \end{pmatrix} \quad \hat{\Sigma}^{imp} = \begin{pmatrix} \Sigma_0 & \Sigma_1 & \Sigma_2 & \Sigma_1 \\ \Sigma_1 & \Sigma_0 & \Sigma_1 & \Sigma_2 \\ \Sigma_2 & \Sigma_1 & \Sigma_0 & \Sigma_1 \\ \Sigma_1 & \Sigma_2 & \Sigma_1 & \Sigma_0 \end{pmatrix} \tag{40}$$

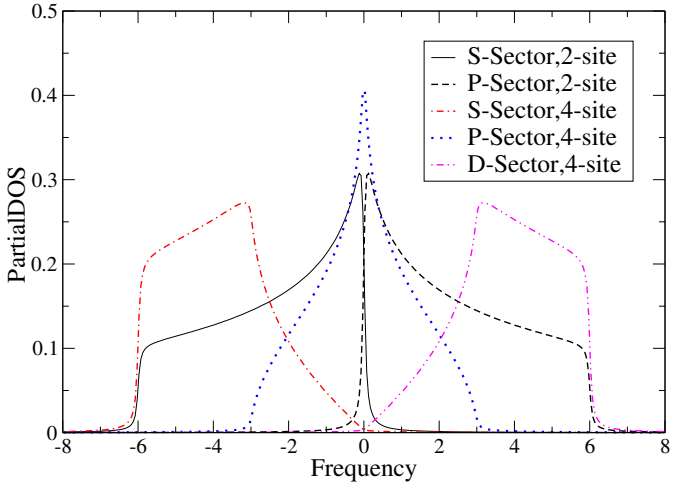

Fig. 6: *The PDOS for 2-site and 4-site DCA partitioning on the square lattice with nearest neighbor hopping. The total bandwidth is 12 which corresponds to the hopping t=1.5. From Ref.[20].*

and the momentum-dependent self energies are

$$\begin{aligned} \Sigma_S &= \Sigma_0 + 2\Sigma_1 + \Sigma_2 \\ \Sigma_P &= \Sigma_0 - \Sigma_2 \\ \Sigma_D &= \Sigma_0 - 2\Sigma_1 + \Sigma_2 \end{aligned} \tag{41}$$

and correspondingly the components of lattice Green's functions are

$$G_{S(P,D)} = \int \frac{D_{S(P,D)}(\epsilon)d\epsilon}{i\omega_n + \mu - \epsilon - \Sigma_{S(P,D)}} \tag{42}$$

The self-consistency equations are

$$\begin{aligned} G_0 &= (G_S + 2G_P + G_D)/4 \\ G_1 &= (G_S - G_D)/4 \\ G_2 &= (G_S - 2G_P + G_D)/4 \end{aligned} \tag{43}$$

We can compare the DCA-partial DOS with a similar consideration for the cluster DMFT [21]. In this case, one first calculate the proper local matrix of the Green functions Eq. (8) and then transform it to the basis of molecular orbitals (inverse of Eqs. (37) and (43)) in order to obtained partial DOS ρ_m (Fig. (7)). It is clear that the DCA partial DOS overestimate "localization" of the partial sectors orbitals ϕ_m while the CDMFT has larger overlap between different partial DOS with non-local Green function contributions. This can lead to spurious k-selective polarization of correlated orbitals in the DCA-scheme compare to the CDMFT method.

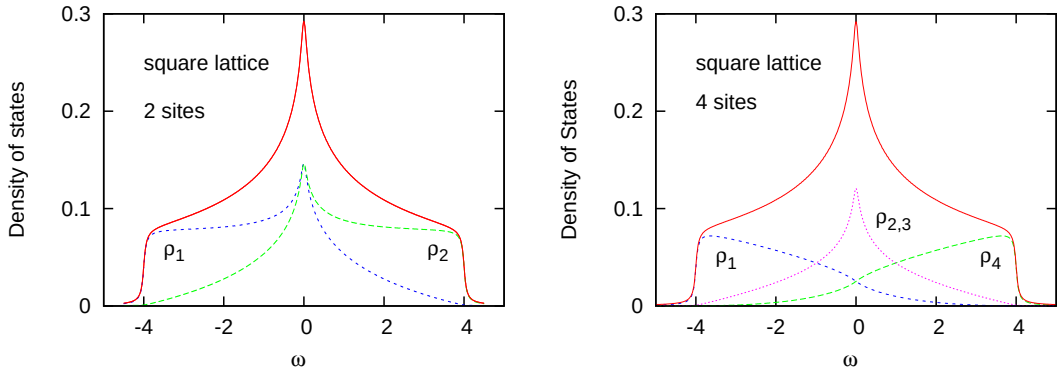

Fig. 7: *Total density of states $\rho(\omega)$ and molecular orbital CDMFT-components $\rho_m(\omega)$ for 2-site (left panel) and 4-site clusters (right panel) of square lattice. The total bandwidth is 8, which corresponds to the hopping t=1. From Ref.[21].*

5 Long-range correlations: Dual-Fermion approach

The shortcomings of cluster DMFT scheme have triggered many efforts to go beyond the mean-field description, while maintaining DMFT as a starting point. The standard DMFT scheme becomes exact in the limit of infinite coordination number z. An expansion in $1/z$, however, leads to difficulties as the action depends in a non-analytic way on the coordination number [22]. Building on earlier work on strong-coupling expansions for the Hubbard model [23, 24, 25], a general framework to perform a systematic cumulant expansion around DMFT even considering non-local Coulomb interaction was developed in Ref. [26].

While cluster extension to DMFT breaks translational symmetry of the lattice, the combination of numerical and analytic methods is a promising route for including the effects of long-range correlations. Recent developments have led to approaches which include long-range correlations via straightforward diagrammatic corrections to DMFT [27, 28, 29]. Based on earlier suggestions for bosonic fields [30], it was recognized that that a systematic, fully renormalized expansion around DMFT can be formulated in terms of auxiliary fermions [31].

Our goal is to find optimal strong-coupling expansion of the general lattice problem described by the imaginary time action

$$S[c^*,c] = -\sum_{\omega\mathbf{k}\sigma\, mm'} c^*_{\omega\mathbf{k}\sigma m}\left[(i\omega+\mu)\mathbf{1} - t^{mm'}_{\mathbf{k}\sigma}\right] c_{\omega\mathbf{k}\sigma m'} + \sum_i S_{\mathrm{U}}[c^*_i, c_i]. \tag{44}$$

Here $t_{\mathbf{k}\sigma}$ is the one-electron part of the Hamiltonian, $\sigma = \uparrow, \downarrow$ labels the spin projection, m, m' are orbital indices and c^*, c are Grassmann variables. The index i labels the lattice sites and k-vectors are quasimomenta. In order to keep the notation simple, it is useful to introduce the combined index $\alpha \equiv \{m\sigma\}$. Translational invariance is assumed for simplicity in the following. For applications it is important to note that the local part of the action, S_{U}, may contain *any* type of local interaction. The only requirement is that it is local within the multi-orbital atom or cluster.

In order to formulate a perturbation expansion around DMFT, a local quantum impurity problem

is introduced:

$$S_{\rm loc}[c^*,c] = -\sum_{\omega\,\alpha\beta} c^*_{\omega\alpha}\left[(i\omega+\mu)\mathbf{1}-\Delta_\omega\right]_{\alpha\beta} c_{\omega\beta} + S_{\rm U}[c^*,c], \tag{45}$$

where Δ_ω is the hybridization matrix describing the coupling of the impurity to an electronic bath. Apart from the connection to DMFT, another motivation for rewriting the lattice action in this form is to express it in terms of a reference problem that can be solved accurately for an arbitrary hybridization function using the CTQMC methods [7]. Exploiting the locality of the hybridization function Δ_ω, the lattice action (44) is rewritten *exactly* by adding and subtracting Δ_ω at each lattice site:

$$S[c^*,c] = \sum_i S_{\rm loc}[c^*_i,c_i] + \sum_{\omega\mathbf{k}\,\alpha\beta} c^*_{\omega\mathbf{k}\alpha}\left(t_\mathbf{k}-\Delta_\omega\right)_{\alpha\beta} c_{\omega\mathbf{k}\beta}. \tag{46}$$

Note that this step leaves the hybridization function unspecified. This will be used later to optimize the approach. The lattice may now be viewed as a collection of impurities, which are coupled through the bilinear term to the right of this equation (see Fig. 8. The effect of spatial correlations enters here and renders an exact solution impossible. A perturbative treatment is desirable, but not straightforward as the impurity action is non-Gaussian and hence there is no Wick theorem. Therefore, dual fermions are introduced in the path integral representation of the partition function from Eq. (6) through the standard Hubbard-Stratonovich transformation

$$\begin{aligned}\exp\left(c^*_\alpha B_{\alpha\beta}(A^{-1})_{\beta\gamma}B_{\gamma\delta}c_\delta\right) = \\ \frac{1}{\det A}\int \mathcal{D}[\gamma^*,\gamma]\exp\left(-f^*_\alpha A_{\alpha\beta}f_\beta - f^*_\alpha B_{\alpha\beta}c_\beta - c^*_\alpha B_{\alpha\beta}f_\beta\right).\end{aligned} \tag{47}$$

In order to transform the exponential of the bilinear term in (46), we choose the matrices a, b in accordance with Refs. [31] as

$$A = g_\omega^{-1}\left(\Delta_\omega - t_\mathbf{k}\right)^{-1} g_\omega^{-1}, \qquad B = g_\omega^{-1}, \tag{48}$$

where g_ω is the local, interacting Green function of the impurity problem. With this choice, the lattice action transforms to

$$S[c^*,c,f^*,f] = \sum_i S_{{\rm site},i} + \sum_{\omega\mathbf{k}\,\alpha\beta} f^*_{\omega\mathbf{k}\alpha}[g_\omega^{-1}\left(\Delta_\omega - t_\mathbf{k}\right)^{-1} g_\omega^{-1}]_{\alpha\beta} f_{\omega\mathbf{k}\beta}. \tag{49}$$

Hence the coupling between sites is transferred to a local coupling to the auxiliary fermions:

$$S_{{\rm site},i}[c^*_i,c_i,f^*_i,f_i] = S_{\rm loc}[c^*_i,c_i] + \sum_{\alpha\beta} f^*_{\omega i\alpha}\, g^{-1}_{\omega\,\alpha\beta} c_{\omega i\beta} + c^*_{\omega i\alpha}\, g^{-1}_{\omega\,\alpha\beta} f_{\omega i\beta}. \tag{50}$$

Since g_ω is local, the sum over all states labeled by $\mathbf{k}$ could be replaced by the equivalent summation over all sites by a change of basis in the second term. The crucial point is that the coupling to the auxiliary fermions is purely local and $S_{\rm site}$ decomposes into a sum of local terms.

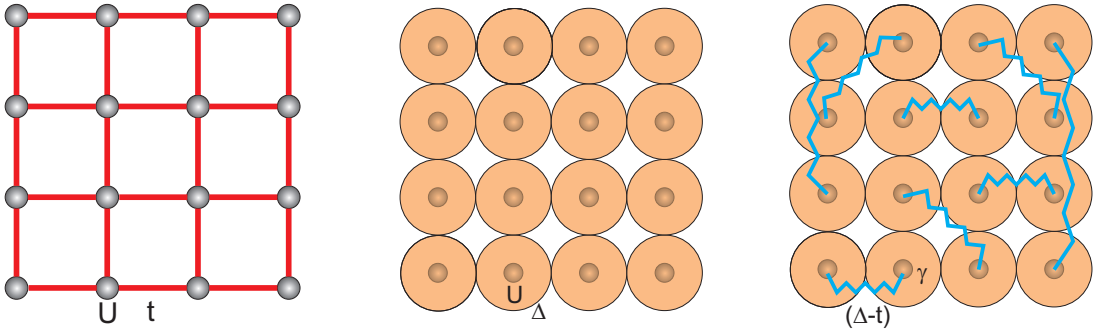

Fig. 8: *Construction of the dual fermion approximation: In a first step, the original lattice problem (left) with bonds (red lines) is replaced by a collection of decoupled impurities exerted to an electronic bath, as indicated by the red spheres (middle), finally spatial correlations in the original lattice problem are treated perturbatively over* $(\Delta_\omega - t_k)$ *(blue wiggly line) with local interaction vertex* γ *(right).*

The lattice fermions can therefore be integrated out from S_{site} for each site i separately. This completes the change of variables:

$$\int \mathcal{D}[c^*, c] \exp\left(-S_{\text{site}}[c_i^*, c_i, f_i^*, f_i]\right) = \mathcal{Z}_{\text{loc}} \exp\Big(- \sum_{\omega\, \alpha\beta} f^*_{\omega i\alpha}\, g^{-1}_{\omega\, \alpha\beta} f_{\omega i\beta} - V_i[f_i^*, f_i]\Big). \tag{51}$$

The above equation may be viewed as the defining equation for the dual potential $V[f^*, f]$. The choice of matrices (48) ensures a particularly simple form of this potential. An explicit expression is found by expanding both sides of Eq. (51) and equating the resulting expressions by order. Formally this can be done up to all orders and in this sense the transformation to the dual fermions is exact. For most applications, the dual potential is approximated by the first non-trivial interaction vertex:

$$V[f^*, f] = \frac{1}{4}\gamma_{1234} f_1^* f_2^* f_4 f_3, \tag{52}$$

where the combined index $1 \equiv \{\omega\alpha\}$ comprises frequency, spin and orbital degrees of freedom. γ is the exact, fully antisymmetric, reducible two-particle vertex of the local quantum impurity problem. It is given by

$$\gamma_{1234} = g^{-1}_{11'} g^{-1}_{22'} \left[\chi_{1'2'3'4'} - \chi^0_{1'2'3'4'}\right] g^{-1}_{3'3} g^{-1}_{4'4}, \tag{53}$$

with the two-particle Green function of the impurity being defined as

$$\chi^{1234} = \langle c_1 c_2 c_3^* c_4^* \rangle_{\text{loc}} = \frac{1}{\mathcal{Z}_{\text{loc}}} \int \mathcal{D}[c^*, c] c_1 c_2 c_3^* c_4^* \exp\Big(- S_{\text{loc}}[c^*, c]\Big). \tag{54}$$

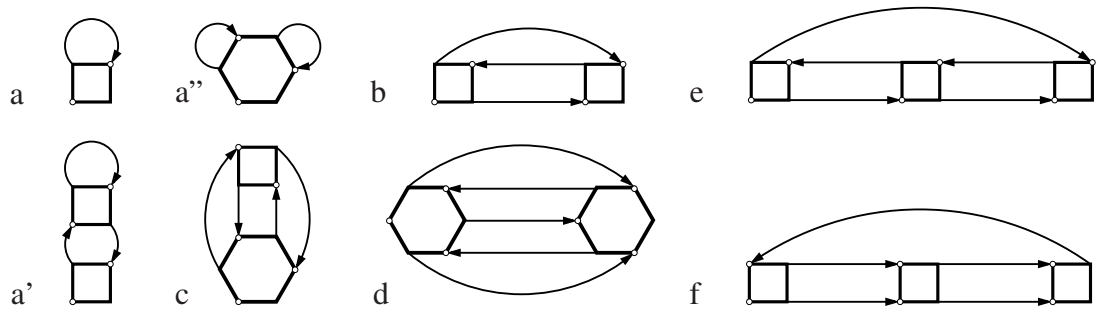

Fig. 9: *Diagrams contributing to the dual self-energy Σ^d. Diagrams a), a'), a") and c) give local, the other ones nonlocal contributions. The three diagrams labeled by a) do not contribute in case the condition (66) is fulfilled. From the Ref. [14].*

The disconnected part reads

$$\chi^0_{1234} = g_{14}g_{23} - g_{13}g_{24}. \tag{55}$$

The single- and two-particle Green functions can be calculated using the CTQMC algorithms [7]. After integrating out the lattice fermions, the dual action depends on the new variables only and reads

$$\tilde{S}[f^*, f] = -\sum_{\omega\mathbf{k}\,\alpha\beta} f^*_{\omega\mathbf{k}\alpha}[\tilde{G}^0_\omega(\mathbf{k})]^{-1}_{\alpha\beta} f_{\omega\mathbf{k}\beta} + \sum_i V_i[f^*_i, f_i]. \tag{56}$$

and the bare dual Green function is found to be

$$\tilde{G}^0_\omega(\mathbf{k}) = -g_\omega \left[g_\omega + (\Delta_\omega - t_\mathbf{k})^{-1}\right]^{-1} g_\omega, \tag{57}$$

which involves the local Green function g_ω of the impurity model.
Up to now, Eqs. (56), (57) are merely a reformulation of the original problem. In practice, approximate solutions are constructed by treating the dual problem perturbatively. Several diagrams that contribute to the dual self-energy are shown in Fig. 9. These are constructed from the impurity vertices and dual Green functions as lines. The first diagram (a) is purely local, while higher orders contain nonlocal contributions, e.g. diagram b). Inserting the renormalized Green function into diagram a) includes contributions such as the one in a'). In practice, approximations to the self-energy are constructed in terms of skeleton diagrams. The lines shown in Fig. 9 are therefore understood to be fully dressed propagators. The use of skeleton diagrams is necessary to ensure the resulting theory to be conserving in the Baym-Kadanoff sense [33], i. e. it fulfills the basic conservation laws for energy, momentum, spin and particle number. It is an important consequence of the exact transformation (47) that for a theory which is conserving in terms of dual fermions, the result is also conserving in terms of lattice fermions [32]. This allows to construct general conserving approximations within the dual fermion approach. Numerically, the self-energy is obtained in terms of skeleton diagrams by performing a self-consistent renormalization as described below. Once an approximate dual self-energy is found, the result may be transformed back to a physical result in terms of lattice fermions using exact relations.

The action (56) allows for a Feynman-type diagrammatic expansion in powers of the dual potential V. The rules are similar to those of the antisymmetrized diagrammatic technique [34]. Extension of these rules to include generic n-particle interaction vertices is straightforward. Due to the use of an antisymmetrized interaction, the diagrams acquire a combinatorial prefactor. For a tuple of n equivalent lines, the expression has to be multiplied by a factor $1/n!$. As simplest example we can write schematically the first self-energy correction of the diagram a) in Fig. 9 contains a single closed loop:

$$\tilde{\Sigma}_{12}^{(a)} = -T\sum_{34}\gamma_{1324}\tilde{G}^{\mathrm{loc}}_{43} \tag{58}$$

where $\tilde{G}^{\mathrm{loc}} = (1/N)\sum_{\mathbf{k}}\tilde{G}(\mathbf{k})$ denotes the local part of the dual Green function. The second-order contribution represented by diagram b) contains two equivalent lines and one closed loop and hence is k-dependence:

$$\tilde{\Sigma}_{12}^{(b)}(\mathbf{k}) = -\frac{1}{2}\left(\frac{T}{N}\right)^2\sum_{\mathbf{k}_1\mathbf{k}_2}\sum_{345678}\gamma_{1345}\tilde{G}_{57}(\mathbf{k}_1)\tilde{G}_{83}(\mathbf{k}_2)\tilde{G}_{46}(\mathbf{k}+\mathbf{k}_2-\mathbf{k}_1)\gamma_{6728} \tag{59}$$

In practice, it is more efficient to evaluate the lowest order diagrams in real space and transform back to reciprocal space using the fast Fourier transform.

5.1 Dual-Fermion approach: Exact relations

After an approximate result for the dual self-energy or the dual Green function has been obtained, it has to be transformed back to the corresponding physical quantities in terms of lattice fermions. The fact that dual fermions are introduced through the exact Hubbard-Stratonovich transformation (47) allows to establish exact identities between dual and lattice quantities. Hence the transformation does not involve any additional approximations [14, 31].

The relations between the n-particle cumulants of dual and lattice fermions can be established using the cumulant (linked cluster) technique. To this end, one may consider two different, equivalent representations of the following generating functional:

$$F[J^*,J;L^*,L] = \ln\,\mathcal{Z}_f\int\mathcal{D}[c^*,c;f^*,f]\exp\Big(-S[c^*,c;f^*,f]+J_1^*c_1+c_2^*J_2 + L_1^*f_1+f_2^*L_2\Big). \tag{60}$$

Integrating out the lattice fermions from this functional similar to (51) (this can be done with the sources J and J^* set to zero) yields

$$F[L^*,L] = \ln\,\tilde{\mathcal{Z}}_f\int\mathcal{D}[f^*,f]\exp\left(-\tilde{S}[f^*,f]+L_1^*f_1+f_2^*L_2\right). \tag{61}$$

with $\tilde{\mathcal{Z}}_f = \mathcal{Z}/\tilde{\mathcal{Z}}$. The dual Green function and two-particle correlator related with non-local susceptibilities are obtained from (61) by suitable functional derivatives, e.g.

$$\tilde{G}_{12} = -\frac{\delta^2 F}{\delta L_2\delta L_1^*}\bigg|_{L^*=L=0},\quad\Big[\tilde{X}-\tilde{G}\otimes\tilde{G}\Big]_{1234} = \frac{\delta^4 F}{\delta L_4\delta L_3\delta L_2^*\delta L_1^*}\bigg|_{L^*=L=0}, \tag{62}$$

where $G \otimes G$ is the antisymmetrized direct product of Green functions, so that the angular brackets is the connected part of the dual two-particle Green function. Conversely, integrating out the dual fermions from (60) using the HST, one obtains an alternative representation, which more clearly reveals a connection of the functional derivatives with respect to the sources J,J^* and L, L^*. The result is

$$F[J^*, J; L^*, L] = L_1^*[g(\Delta - h)g]_{12} L_2 + \ln \int \mathcal{D}[c^*, c] \exp\Big(- S[c^*, c] + \\ + J_1^* c_1 + c_2^* J_2 + L_1^*[g(\Delta - t)]_{12} c_2 + c_1^*[(\Delta - t)g]_{12} L_2 \Big). \tag{63}$$

In analogy to (62), the cumulants in terms of lattice fermions are obviously obtained by functional derivative with respect to the sources J and J^* with L and L^* set to zero. Applying the derivatives with respect to L, L^* to (63) with $J = J^* = 0$ and comparing to (62), e.g. yields the following identity:

$$\tilde{G}_{12} = -[g(\Delta - t)g]_{12} + [g(\Delta - t)]_{11'} G_{1'2'} [(\Delta - t)g]_{2'2}. \tag{64}$$

Solving for G provides the rule how to transform the dual Green function to the physical quantity in terms of lattice fermions. For higher-order cumulants the additive term in (63) does not contribute and the relation between the two-particle cumulants evaluates to

$$\left[\tilde{X} - \tilde{G} \otimes \tilde{G}\right]_{1234} = \\ [g(\Delta - t)]_{11'} \, [g(\Delta - t)]_{22'} \, [X - G \otimes G]_{1'2'3'4'} \, [(\Delta - t)g]_{3'3} \, [(\Delta - t)g]_{4'4} \,, \tag{65}$$

It is apparent that similar relations hold for higher-order cumulants. Note that the transformation only involves single-particle functions. Hence one may conclude that n-particle collective excitations are the same for dual and lattice fermions.

5.2 Self-consistency condition and relation to DMFT

The hybridization function Δ, which so far has not been specified, allows to optimize the starting point of the perturbation theory and should be chosen in an optimal way. The condition of the first diagram (Fig. 9 a) in the expansion of the dual self-energy to be equal to zero at all frequencies fixes the hybridization. This eliminates the leading order diagrammatic correction to the self-energy and establishes a connection to DMFT, which can be seen as follows: Since γ vertex is local, this condition amounts to demanding that the local part of the dual Green function be zero:

$$\sum_{\mathbf{k}} \tilde{G}_\omega(\mathbf{k}) = 0. \tag{66}$$

The simplest nontrivial approximation is obtained by taking the leading-order correction, diagram a), evaluated with the bare dual propagator (57). Recalling the expression for the DMFT Green function, Eq. (4), it is readily verified that

$$G_\omega^{\mathrm{DMFT}}(\mathbf{k}) - g_\omega = \left[g_\omega^{-1} + \Delta_\omega - t_{\mathbf{k}}\right]^{-1} - g_\omega \\ = -g_\omega \left[g_\omega + (\Delta_\omega - t_{\mathbf{k}})^{-1}\right]^{-1} g_\omega = \tilde{G}_\omega^0(\mathbf{k}). \tag{67}$$

It immediately follows that (66) evaluated with the bare dual Green function is exactly equivalent to the DMFT self-consistency condition:

$$\frac{1}{N}\sum_{\mathbf{k}} \tilde{G}^0_\omega(\mathbf{k}) = 0 \quad \Longleftrightarrow \quad \frac{1}{N}\sum_{\mathbf{k}} G^{\mathrm{DMFT}}_\omega(\mathbf{k}) = g_\omega. \tag{68}$$

Hence DMFT appears as the zero-order approximation in this approach and corrections to DMFT are included perturbatively. A formal relation to DMFT can be established using the Feynman variational functional approach. In this context, DMFT appears as the optimal approximation to a Gaussian ensemble of dual fermions [32].

When diagrammatic corrections are taken into account and the first diagram is evaluated with the dressed propagator $\tilde{G}$, the condition (66) will in general be violated. It can be reinforced by adjusting the hybridization function iteratively. This corresponds to eliminating an infinite partial series starting from the diagrams labeled by a) in Fig. 9. These contributions are effectively absorbed into the impurity problem. Note that such an expansion is not one around DMFT, but rather around an optimized impurity problem.

The only difference between a DMFT and a DF calculation are the diagrammatic corrections which are included into the dual Green function. To this end, the local impurity vertex γ has to be calculated in addition to the Green function in the impurity solver step.

Since the choice of the hybridization function is not unique, one may replace it by a discrete version $\Delta^{(n)} = \sum_{k=1}^{n} |V_k|^2/(i\omega - \epsilon_{\mathbf{k}})$ for a small number n of bath degrees of freedom, for which the impurity problem can be solved efficiently using exact diagonalization. In this case, the condition (66) cannot be fulfilled in general, but one may require the correction to be *minimal* instead. This results in a variational approach. The corresponding perturbation expansion is considerably more stable than an expansion around the atomic limit, i.e. $\Delta \equiv 0$ [24].

5.3 Results for the 2d-Hubbard model

In the following, we show some illustrative results for the Hubbard model, which is governed by the Hamiltonian (1). Unless otherwise stated, only the two lowest-order diagrams a) and b) of Fig. 9 have been used. It may be considered as a benchmark system for the approach, because the importance of nonlocal correlations is expected to increase by reducing the dimensionality. This is clearly an unfavorable situation for DMFT, which completely neglects spatial correlations.

In order to visualized the nonlocal correlations, the k-dependent self-energy is shown in Fig. (10). The upper panel of Figure 10 presents contour plots for $\mathrm{Im}\Sigma_{\omega=0,k}$ at $U = 1.0$ and $U = 2.0$ (the data are obtained by a polynomial extrapolation from the Matsubara frequencies). The value of $\mathrm{Im}\Sigma_{\omega=0,k}$ grows dramatically as U changes from 1.0 to 2.0. Close to the Mott transition there is a strong k-dependence of Σ. The renormalized dispersion law $\epsilon_k + \mathrm{Re}\Sigma_{\omega=0,k}$ is now also in a qualitative agreement with numerical data, as the lower panel of Figure 10. In these graphs, $\epsilon_k + \mathrm{Re}\Sigma_{\omega=0,k}$ is compared with the reference data for a 10×10 lattice. There is a qualitative difference between the results for $U = 1.0$ and $U = 2.0$: for later case the corrections are quite large so that there is a dependence resembling ϵ_k^{-1} [31, 31].

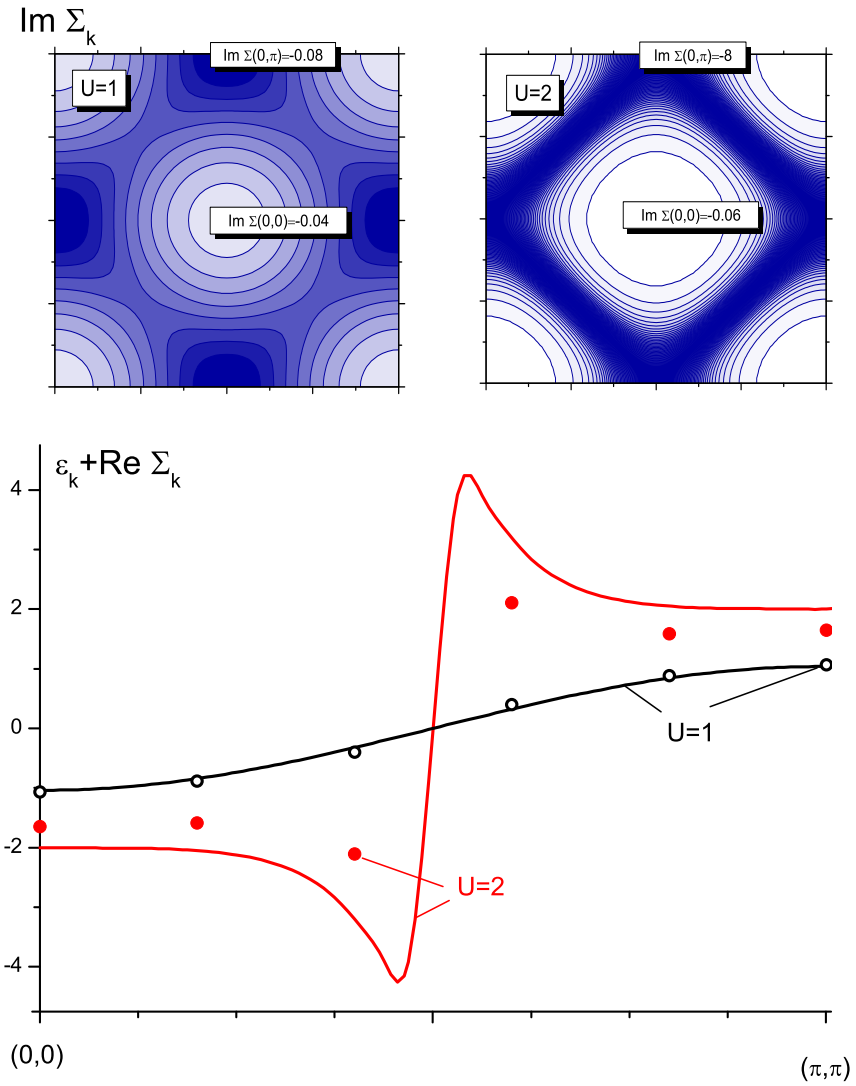

Fig. 10: *Momentum dependence for the self-energy function at Fermi energy, obtained with diagram (b) within the translationally-invariant approximation for the undoped Hubbard model. Data are shown at* $t = 0.25, \beta = 20$, *for* $U = 1.0$ *and* $U = 2.0$. *Upper panel: contour plots for* k*-dependence of the imaginary part of the self energy. Lower panel: renormalized dispersion law* $\epsilon_k + \mathrm{Re}\Sigma_{\omega=0,k}$, *compared with the reference data obtained for* 10×10 *lattice. From the Ref. [31].*

The k-resolved spectral function $A(\mathbf{k}, \omega)$ obtained from maximum-entropy analytical continuation shown in Fig. 11. The DMFT spectral function displays a quasiparticle band, while in the DF calculation, spectral weight is transferred away from the Fermi level. Recalling the nesting condition $\epsilon_{\mathbf{k}+\mathbf{Q}} = -\epsilon_{\mathbf{k}}$ for the antiferromagnetic wave vector $\mathbf{Q} = (\pi, \pi)$, the locus of these features allows to interpret them as shadow bands due to dynamical short-range antiferromagnetic correlations. The strength of these correlations increases as the temperature is lowered.

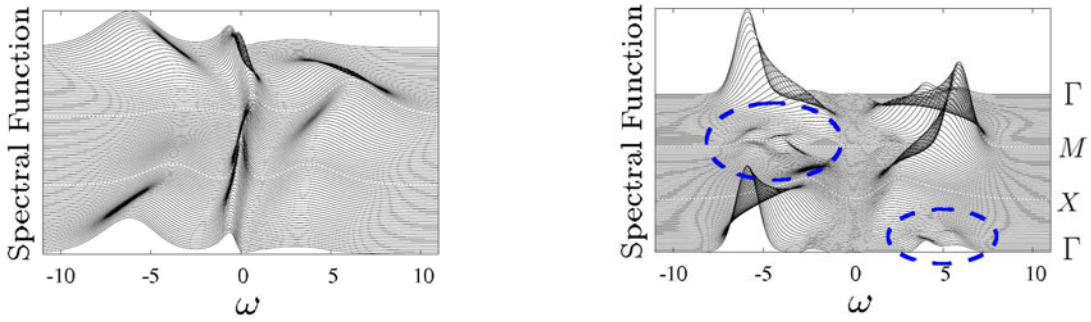

Fig. 11: *Spectral function $A(\mathbf{k},\omega)$ for the 2D Hubbard model at half-filling obtained within DMFT (left) and dual fermion calculations (right) for $U = 8t$ and $T/t = 0.235$. From bottom to top, the curves are plotted along the high-symmetry lines $\Gamma \to X \to M \to \Gamma$. The high-symmetry points $X = (0,\pi)$ and $M = (\pi,\pi)$ are marked by dashed lines. The structures encircled in blue can be attributed to dynamical short-range antiferromagnetic correlations. From the Ref. [14].*

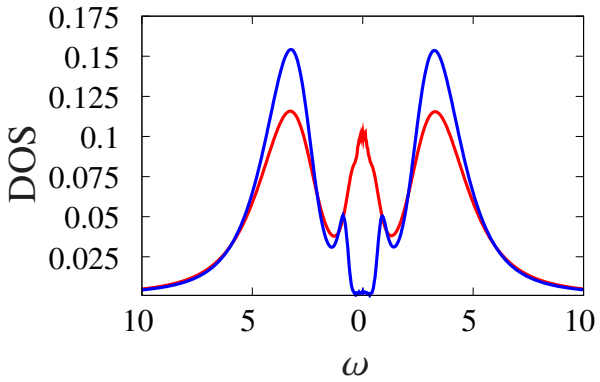

Fig. 12: *Metallic and insulating local density of states obtained in the coexistence region of the Mott transition for $U/t = 6.5$ and $T/t = 0.08$. The insulating solution exhibits characteristic peaks at the gap edge. The antiferromagnetic correlations lead to antiferromagnetic-gap-like behavior [35]. The metallic solution exhibits shoulders on the peak at the Fermi level. From the Ref. [14].*

A detailed analysis of the phasediagram shows that these correlations lead to a drastic reduction of the critical U from $U_c/t \sim 9.35$ in DMFT down to $U_c/t \sim 6.5$ within the dual fermion calculation. This, as well as the density of states in the coexistence region (Fig. 12) and the slope of the transition lines in the $U - T$ phase diagram below the critical point, which are modified from negative within DMFT to positive [14], is in qualitative agreement with cluster DMFT results [36]. We emphasize that these results cannot be obtained from a straightforward diagrammatic expansion around DMFT as the modification of the Weiss field is essential. This distinguishes the present method from related approaches [28, 29].

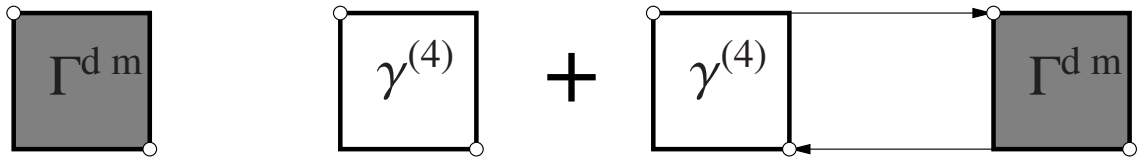

Fig. 13: *Bethe-Salpeter equation for the dual vertex in the electron-hole channel with a local approximation $\Gamma_{irr} = \gamma$ to the irreducible vertex. The solution Γ contains the sum of all ladder diagrams up to infinite order in γ.*

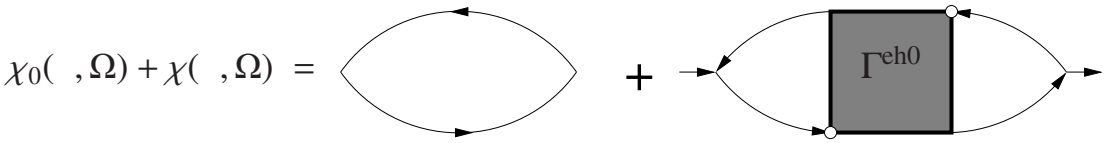

Fig. 14: *Diagrammatic representation of the susceptibility, Eqs. (71), (72).*

5.4 Calculation of susceptibilities

For the calculation of the dual susceptibility, the dual vertex function is first calculated by means of a Bethe-Salpeter equation [37, 38] (in the following we write the equations for a single-orbital model for simplicity)

$$\Gamma^{\alpha}_{\omega\omega'\Omega}(\mathbf{q}) = \gamma^{\alpha}_{\omega\omega'\Omega} - \frac{T}{N}\sum_{\omega''}\sum_{\mathbf{k}} \gamma^{\alpha}_{\omega\omega''\Omega}\tilde{G}_{\omega''}(\mathbf{k})\tilde{G}_{\omega''+\Omega}(\mathbf{k}+\mathbf{q})\,\Gamma^{\alpha}_{\omega''\omega'\Omega}(\mathbf{q}). \tag{69}$$

This equation is depicted diagrammatically in Fig. 13. Here the irreducible vertex is approximated by the local irreducible interaction of dual fermions to lowest-order and is hence given by the *reducible* vertex of the impurity model γ (the index '(4)' is omitted in what follows). Here $\alpha = \mathrm{d}, \mathrm{m}$ stands for the density (d) and magnetic (m) electron-hole channels: $\Gamma^{\mathrm{d}} = \Gamma^{\uparrow\uparrow\uparrow\uparrow} + \Gamma^{\uparrow\uparrow\downarrow\downarrow}$, $\Gamma^{\mathrm{m}} = \Gamma^{\uparrow\uparrow\uparrow\uparrow} - \Gamma^{\uparrow\uparrow\downarrow\downarrow}$. The physical content of the BSE is repeated scattering of particle-hole pairs. In the two channels the particle-hole pair has a definite total spin S and spin projection S_z. The density channel corresponds to the $S = 0$, $S_z = 0$ singlet channel, while Γ^{m} is the vertex in the $S = 1$, $S_z = 0$ triplet channel. In the magnetic channel, the collective excitations are magnons. The vertex $\Gamma^{\uparrow\downarrow\downarrow\uparrow}$ ($\Gamma^{\downarrow\uparrow\uparrow\downarrow}$) which corresponds to the $S_z = +1(-1)$ spin projection of the $S = 1$ channel must be equal to Γ^{m} in the paramagnetic state (longitudinal and transverse modes cannot be distinguished).

The BSE may be solved iteratively, starting from the approximation $\Gamma^{(0)} \approx \gamma$. Inserting this into the right-hand-side of Eq. (69) yields a new approximation $\Gamma^{(1)}$. Repeating this step successively generates a sum of all ladder diagrams with $1, \ldots, n+1$ irreducible rungs in the

approximation $\Gamma^{(n)}$. In practice however, the BSE is solved by matrix inversion according to

$$[\Gamma^{\alpha}_{\omega\omega'\Omega}(\mathbf{q})]^{-1} = (\gamma^{\alpha}_{\omega\omega'\Omega})^{-1} + \frac{T}{N}\sum_{\mathbf{k}} \tilde{G}_{\omega}(\mathbf{k})\tilde{G}_{\omega+\Omega}(\mathbf{k}+\mathbf{q})\delta_{\omega\omega'} \ , \tag{70}$$

which corresponds to summing up the infinite series. The vertices are matrices in the fermionic Matsubara frequencies ω, ω'. They are diagonal with respect to Ω and $\mathbf{q}$, since the center of mass energy and momentum of the particle-hole pair is conserved in scattering processes.
From the vertex, the non-local spin and charge susceptibility is finally obtained as $X = X_0 + X_1$, where

$$X_0(\mathbf{q},\Omega) = -\frac{T}{N}\sum_{\omega}\sum_{\mathbf{k}} G_{\omega}(\mathbf{k})G_{\omega+\Omega}(\mathbf{k}+\mathbf{q}) \tag{71}$$

and

$$X_1^{\alpha}(\mathbf{q},\Omega) = \frac{T^2}{N^2}\sum_{\omega\omega'}\sum_{\mathbf{k}\mathbf{k}'} G_{\omega}(\mathbf{k})G_{\omega+\Omega}(\mathbf{k}+\mathbf{q})\Gamma^{\alpha}_{\omega\omega'\Omega}G_{\omega'}(\mathbf{k}')G_{\omega'+\Omega}(\mathbf{k}'+\mathbf{q}). \tag{72}$$

In principle, these relations are valid for dual and lattice fermions. If one is only interested in instabilities, which are signalled by the divergence of the corresponding susceptibility , it is sufficient to consider the dual quantities. The equivalence of two-particle excitations in terms of dual and lattice fermions ensures that the dual and lattice susceptibilities diverge at the same parameters. The lattice susceptibility is obtained using the exact relations between dual and lattice correlation functions (65). In the context of DMFT, the susceptibility is obtained using relations similar to Eqs. (69), (71) and (72) [2]. The momentum dependence of the irreducible vertex is neglected in DMFT. It is further approximated by the irreducible vertex of the impurity model. Recall that the lattice Green function is exactly equal to the DMFT Green function when dual corrections to the self-energy are neglected and the dual Green function fulfills the self-consistency condition (66). Using the relation between the DMFT and bare dual Green function Eq. (67) we can find a simple relations between the bare susceptibilities:

$$\tilde{X}_0(\mathbf{q},\Omega) = X_0(\mathbf{q},\Omega) - \chi_0(\Omega). \tag{73}$$

It is an important property of the above equations that under the same conditions the lattice susceptibility calculated within the dual fermion approach is exactly equal to the DMFT susceptibility [14].
As a further illustration, we plot the dynamical susceptibility $\chi(\mathbf{q},\omega)$ in Fig. 15. It clearly displays the magnon spectrum in the paramagnetic state. The dispersion from spin wave theory is shown for comparison. It is given by the expression [39] $\epsilon(\mathbf{k}) = 2zJS\sqrt{1-\gamma(\mathbf{k})^2}$ where z is the coordination number, $S = 1/2$ is the spin of the fermions and $\gamma(\mathbf{k}) = \frac{1}{z}\sum_{\mathrm{NN}} e^{i\mathbf{k}\mathbf{r}_{\mathrm{NN}}} = (\cos k_x + \cos k_y)/2$ for the square lattice. The right panel of Fig. 15 shows a cross-section for the antiferromagnetic wave vector $\mathbf{q}_{\mathrm{AF}} = (\pi,\pi)$ (M-point). The peak is broadened and slightly shifted from zero. Such a behavior is reminiscent of a 2D Heisenberg model at finite temperature, where long-range order with a correlation length $\xi \gg a$ takes place (a is the lattice constant) and a corresponding small energy scale of order Ja/ξ arises [35].

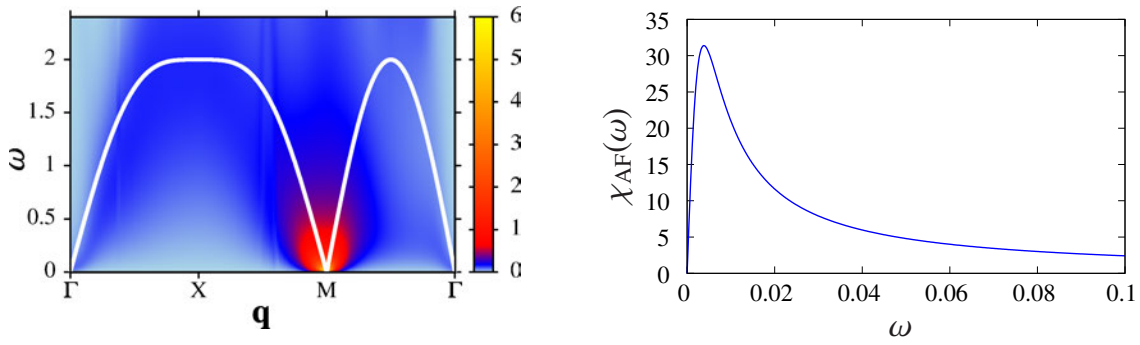

Fig. 15: *Left: Dynamical susceptibility $\chi(\mathbf{q},\omega)$ for $U/t = 4$ and $T/t = 0.19$, obtained from a dual fermion calculation and analytical continuation using Padé approximants. It shows the magnon spectrum in the paramagnetic state. The dispersion from spin wave theory with effective exchange coupling $J = 4t^2/U$ is shown for comparison. Values for $\chi > 6$ are excluded from the colormap to improve the contrast. Right: Cross-section through the peak at the M-point. The displacement from zero is consistent with a small energy scale J/ξ, where ξ is the correlation length (in units of the lattice constant). From the Ref. [14].*

5.5 Convergence properties

For a perturbative approach, the convergence properties are of paramount importance. For the present theory[41], the vertices appear as a small parameter in the expansion in the weak-coupling limit ($U \to 0$), because they vanish at least proportionally to U: $\gamma^{(4)} \sim U$, $\gamma^{(6)} \sim U^2$,.... On the other hand, for an expansion around the atomic limit ($\Delta \equiv 0$), the dual Green function is small near this limit: For $h_{\mathbf{k}}$ small, the bare dual Green function can be approximated as

$$\tilde{G}^0_\omega(\mathbf{k}) \approx g_\omega \, h_{\mathbf{k}} \, g_\omega. \tag{74}$$

This enforces the convergence of the series in the opposite strong coupling limit. In contrast, IPT or FLEX, which operate with the bare interaction U, have to break down at intermediate to large U. In the general case, a fast convergence cannot be proven rigorously. Here we examine the convergence properties numerically in the vicinity of the antiferromagnetic instability (AFI) in the 2D Hubbard model. These can be characterized using the eigenvalue problem derived from the BSE (69).

The matrix is the building block of the particle-hole ladder and may be thought of as the effective two-fermion interaction. For dual fermions, the irreducible vertex is given by the bare dual interaction $\Gamma^{\text{irr, m}}_{\omega\omega'\Omega} = \gamma^{\text{m}}_{\omega\omega'\Omega} = \gamma^{\uparrow\uparrow}_{\omega\omega'\Omega} - \gamma^{\uparrow\downarrow}_{\omega\omega'\Omega}$ in the magnetic channel and $\tilde{G}$ stands for the full dual Green function. Here the focus is on the leading eigenvalues in the vicinity of the AFI and hence $\mathbf{q} = (\pi,\pi)$ and $\Omega = 0$. An eigenvalue of $\lambda_{\text{max}} = 1$ implies a divergence of the ladder sum and hence a breakdown of the perturbation theory.

$$-\frac{T}{N}\sum_{\omega'\mathbf{k}'} \Gamma^{\text{irr, m}}_{\omega\omega'\Omega}\tilde{G}_{\omega'}(\mathbf{k})\tilde{G}_{\omega'+\Omega}(\mathbf{k}+\mathbf{q})\,\phi_{\omega'} = \tilde{\lambda}\phi_{\omega'}. \tag{75}$$

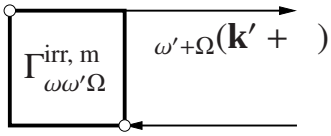

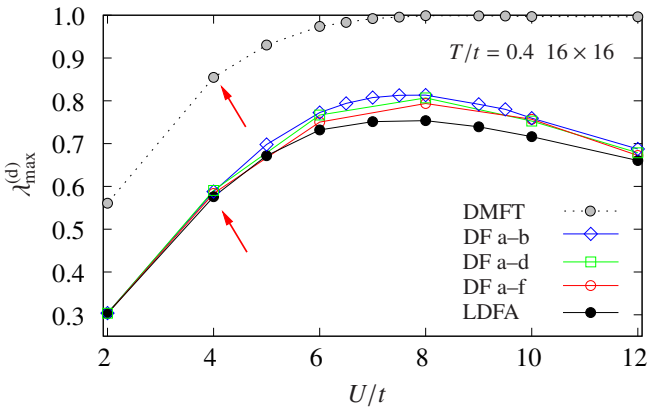

Fig. 16: *Leading eigenvalue of the Bethe-Salpeter equation obtained within various approximations in the* $\mathbf{q} = (\pi, \pi)$ *magnetic channel as a function of the interaction* U*.* λ *(*λ^d*) denotes lattice (dual) fermion eigenvalues. The diagrams included are indicated in the legend (labels are the same as in Fig. 9). The dual perturbation theory converges fast (i.e. the eigenvalues are small) in particular for weak and strong coupling. A straightforward diagrammatic expansion around DMFT breaks down for large* U*. From the Ref. [41].*

The results are displayed in Fig. 16. For weak coupling, the leading eigenvalue is small and implies a fast convergence of the diagrams in the electron-hole ladder. More significantly, the eigenvalues decrease and converge to the same intercept in the large U limit. This nicely illustrates that the dual perturbation theory smoothly interpolates between a standard perturbation expansion at small, and the cumulant expansion at large U, ensuring fast convergence in both regimes. From the figure it is clear that this also improves the convergence properties for intermediate coupling ($U \sim W$). Even here corrections from approximations involving higher-order diagrams remain small, including those from the LDFA. Diagrams involving the three-particle vertex give a negligible contribution.

For a straightforward diagrammatic expansion around DMFT, the building block of the particle-hole ladder is constructed from the irreducible impurity vertex $\gamma^{\mathrm{irr,\,m}}_{\omega\omega'\Omega}$ and DMFT Green functions. As seen in Fig. 16, the corresponding leading eigenvalue (and the effective interaction) is much larger than for dual fermions over the whole parameter range (e.g. at red arrows). When transforming the leading eigenvalue back to lattice fermions, it is close to the DMFT value for these parameters. Hence convergence is enhanced for a perturbation theory in terms of dual fermions. Remarkably, for the intermediate to strong coupling region, a straightforward perturbation theory around DMFT breaks down (since the eigenvalue approaches one), while for a theory in terms of dual fermions, this is not the case. The fact that the leading eigenvalue for dual fermions is smaller is a generic feature. It is also observed away from half-filling and for the electron-electron channel. Note that the interaction in the dual fermion approach is given by the reducible vertex of the impurity. The frequency dependence accounts for the fact that the Coulomb interaction acts on short time scales in this approach. Strong local correlations are effectively separated (and treated non-perturbatively within the solution of the impurity model) from weaker spatial correlations, which are treated diagrammatically.

6 Summary and outlook

Different cluster extensions of the DMFT scheme are very useful tools to describe non-local short-range correlations in solids. The solution of the effective multi-site cluster impurity problem in fermionic bath is a common feature of CDMFT and DCA methods and can be can be found within numerically exact CTQMC approach. Nevertheless all cluster extension of the DMFT have problems: while CDMFT breaks translational symmetry of crystals, DCA effectively renormalized lattice hopping and makes a step-like momentum dependence of self-energy. We still should find an optimal way of periodization the CDMFT scheme. For the DCA approach one can average over different tiling of the Brillouin zone within the same cluster as was suggested for non-local CPA scheme [9]. For the CDMFT scheme the main problem is to find periodic self-energy solution, which preserve the analytical properties of the lattice Green's function [16]. In this case, even for small clusters one can find a similar solution for both CDMFT and DCA methods.

The dual fermion scheme gives a general framework to include non-local correlations on all scales. The bottleneck of DF-scheme related with finite number of diagrams which one can calculate, and the accuracy of short-range correlations are not as good as in numerically exact cluster solution. There are straightforward generalizations of the single site DF-approach to the cluster dual fermion approach (CDFA)[40] as well as DFDCA-scheme [42]. We can think that the cluster DMFT starting point will allow to find a better non-local solutions, which have exact short-range correlations and reasonable long-range correlations. This may be an optimal way to study the complicated non-local effects in solids.

Acknowledgment

Support of the Deutsche Forschungsgemeinschaft through FOR1346 is gratefully acknowledged.

References

[1] G. Kotliar and D. Vollhardt, Physics Today **57**, 53 (2004)

[2] A. Georges, G. Kotliar, W. Krauth, and M.J. Rozenberg, Rev. Mod. Phys. **68** , 13 (1996)

[3] V.I. Anisimov, A.I. Poteryaev, M.A. Korotin, A.O. Anokhin, and G. Kotliar, J. Phys.: Condensed Matter **9**, 7359 (1997)

[4] A.I. Lichtenstein and M.I. Katsnelson, Phys. Rev. B **57**, 6884 (1998)

[5] G. Kotliar, S.Y. Savrasov, K. Haule, V.S. Oudovenko, O. Parcollet, and C.A. Marianetti, Rev. Mod. Phys. **78**, 865 (2006)

[6] A.I. Lichtenstein and M.I. Katsnelson, Phys. Rev. B **62**, R9283 (2000)

[7] E. Gull, A.J. Millis, A.I. Lichtenstein, A.N. Rubtsov, M. Troyer, and P. Werner, Rev. Mod. Phys. **83**, 349 (2011)

[8] G. Kotliar, S.Y. Savrasov, G. Palsson, and G. Biroli, Phys. Rev. Lett. **87**, 186401 (2001)

[9] D.A. Rowlands, X.-G. Zhang, and A. Gonis, Phys. Rev. B **78**, 115119 (2008)

[10] T. Maier, M. Jarrell, T. Pruschke, and M.H. Hettler, Rev. Mod. Phys. **77**, 1027 (2005)

[11] M. Potthoff, M. Aichhorn, and C. Dahnken, Phys. Rev. Lett. **91**, 206402 (2003)

[12] A. Fuhrmann, S. Okamoto, H. Monien, and A.J. Millis, Phys. Rev. B **75**, 205118 (2007)

[13] S. Okamoto, A.J. Millis, H. Monien, and A. Fuhrmann, Phys. Rev. B **68**, 195121 (2003)

[14] H. Hafermann: *Numerical Approaches to Spatial Correlations in Strongly Interacting Fermion Systems* (Cuvillier Verlag, Göttingen, Singapore, 2010)

[15] G. Biroli and G. Kotliar, Phys. Rev. B **65**, 155112 (2002)

[16] G. Biroli. O. Parcollet and G. Kotliar, Phys. Rev. B **69**, 205108 (2004)

[17] E. Koch, G. Sangiovanni, and O. Gunnarsson, Phys. Rev. B **78**, 115102 (2008)

[18] M. Potthoff, Eur. Phys. J. B **32**, 429 (2003)

[19] M. Potthoff and M. Balzer, Phys. Rev. B **75**, 125112 (2007)

[20] C. Lin and A.J. Millis, Phys. Rev. B **79**, 205109 (2009)

[21] A. Liebsch, H. Ishida, J. Merino, Phys. Rev. B **78**, 165123 (2008)

[22] A. Schiller and K. Ingersent, Phys. Rev. Lett. **75**, 113 (1995)

[23] S. Pairault, D. Sénéchal, and A.-M.S. Tremblay, Phys. Rev. Lett. **80**, 5389 (1998)

[24] S. Pairault, D. Sénéchal, and A.-M.S. Tremblay, European Phys. Journal B **16**, 85 (2000)

[25] S.K. Sarker, J. Physics C: Solid State Phys. **21**, L667 (1988)

[26] T.D. Stanescu and G. Kotliar, Phys. Rev. B **70**, 205112 (2004)

[27] C. Slezak, M. Jarrell, Th. Maier, and J. Deisz, J. Phys.: Condens. Matter **21**, 435604 (2009)

[28] A. Toschi, A.A. Katanin, and K. Held, Phys. Rev. B **75**, 045118 (2007)

[29] H. Kusunose, J. Phys. Soc. Japan **75**, 054713 (2006)

[30] A.N. Rubtsov, Phys. Rev. B **66**, 052107 (2002)

[31] A.N. Rubtsov, M.I. Katsnelson, and A.I. Lichtenstein, Phys. Rev. B **77**, 033101 (2008)

[32] A.N. Rubtsov, M.I. Katsnelson, A.I. Lichtenstein, and A. Georges, Phys. Rev. B **79**, 045133 (2009)

[33] G. Baym and L.P. Kadanoff, Phys. Rev. **124**, 287 (1961)

[34] A.A. Abrikosov, L.P. Gorkov, and I.E. Dzyaloshinskii: *Methods of Quantum Field Theory in Statistical Physics* (Pergamon Press, New York, 1965)

[35] V.Y. Irkhin and M.I. Katsnelson, J. Phys.: Cond. Matter **3** 3, 6439 (1991)

[36] H. Park, K. Haule, and G. Kotliar, Phys. Rev. Lett. **101**, 186403 (2008)

[37] A.B. Migdal: *Theory of Finite Fermi Systems and applications to atomic nuclei* (Interscience Publishers, New York, 1967)

[38] P. Nozières: *Theory of interacting Fermi systems* (Benjamin, New York, 1964).

[39] A. Auerbach: *Interacting Electrons and Quantum Magnetism* (Springer, New York, 1998).

[40] H. Hafermann, S. Brener, A.N. Rubtsov, M.I. Katsnelson, A.I. Lichtenstein, JETP Lett. **86**, 677 (2007)

[41] H. Hafermann, G. Li, A.N. Rubtsov, M.I. Katsnelson, A.I. Lichtenstein, and H. Monien, Phys. Rev. Lett. **102**, 206401 (2009)

[42] S.-X. Yang, H. Fotso, H. Hafermann, K.-M. Tam, J. Moreno, T. Pruschke, and M. Jarrell, arXiv:1104.3854